

Accelerated spin-adapted ground state preparation with non-variational quantum algorithms

Takumi Kobori^{1,*}, Taichi Kosugi^{2,1}, Hirofumi Nishi^{2,1}, Synge Todo^{1,3,4} and Yu-ichiro Matsushita^{1,2,5}

¹*Department of Physics, The University of Tokyo, Tokyo 113-0033, Japan*

²*Quemix Inc., Taiyo Life Nihombashi Building, 2-11-2, Nihombashi Chuo-ku, Tokyo 103-0027, Japan*

³*Institute for Physics of Intelligence, The University of Tokyo, Tokyo 113-0033, Japan*

⁴*Institute for Solid State Physics, The University of Tokyo, Kashiwa 277-8581, Japan*

⁵*Quantum Materials and Applications Research Center,
National Institutes for Quantum Science and Technology (QST),
2-12-1 Ookayama, Meguro-ku, Tokyo 152-8550, Japan*

(Dated: June 6, 2025)

Various methods have been explored to prepare the spin-adapted ground state—the lowest energy state within the Hilbert space constrained by externally specified values of the total spin magnitude and the spin- z component. In such problem settings, variational and non-variational methods commonly incorporate penalty terms into the original Hamiltonian to enforce the desired constraints. While in variational approaches, only $O(n_{\text{spin}}^2)$ measurements are required for the calculation of the penalty terms for the total spin magnitude, non-variational approaches, such as probabilistic imaginary-time evolution or adiabatic time evolution, are expected to be more computationally intensive, requiring $O(n_{\text{spin}}^4)$ gates naively. This paper proposes a new procedure based on non-variational quantum algorithms to obtain the spin-adapted ground state. The proposed method consists of two steps: the first step is to prepare a spin-magnitude adapted state and the second step is post-processing for the desired S_z . By separating into two steps, the procedure achieves the desired spin-adapted ground state while reducing the number of penalty terms from $O(n_{\text{spin}}^4)$ to $O(n_{\text{spin}}^2)$. We conducted numerical experiments for spin-1/2 Heisenberg ring models and manganese trimer systems. The results confirmed the effectiveness of our method, demonstrating a significant reduction in gate complexity and validating its practical usefulness.

I. INTRODUCTION

Exploration of complex spin systems plays a crucial role in deepening our understanding of quantum many-body physics [1]. Quantum computers offer a promising platform for efficiently simulating such systems by leveraging their ability to represent the exploration space using qubits proportional to the system size [2–5]. As a result, the development of quantum algorithms for these tasks has been an active area [6–10]. Among these, various methods have been proposed for preparing the ground state of quantum spin systems on quantum computers [11–21]. In particular, considerable attention has been directed toward preparing spin-adapted ground states, which correspond to the lowest-energy eigenstates within Hilbert subspaces constrained to fixed values of the total spin magnitude and spin- z component. The explorations of such spin-restricted Hilbert subspaces are crucial for obtaining a more detailed and accurate understanding of problems in condensed matter physics and quantum chemistry [22–26].

Methods for calculating the spin-adapted ground state can generally be classified into variational and non-variational approaches [13, 27–31]. In variational approaches, one common method involves adopting an objective function that includes penalty terms added to the original Hamiltonian [29, 30]. The penalty terms for

the total spin magnitude are typically proportional to $(\langle \hat{S}^2 \rangle - s^*(s^* + 1))^2$, where s^* is the target value for total spin magnitude, and are generally more computationally demanding than those for spin- z . Although the expression involves a fourth-order polynomial in \hat{S} , the number of measurements required scales as $O(n_{\text{spin}}^2)$, even under the worst-case encoding for a system of n_{spin} spins to compute the expectation value of \hat{S}^2 from the measurement outcomes. This indicates that variational approaches remain efficient in terms of measurement cost when incorporating such penalty terms. However, they require a classical optimization process for parameterized circuits, which can be computationally demanding and prone to convergence issues such as local minima and barren plateaus [32].

On the other hand, non-variational approaches, such as probabilistic imaginary-time evolution (PITE) [18, 33–35] and adiabatic time evolution (ATE) [14, 27, 36], do not rely on parameterized circuits and are particularly appealing in fault-tolerant quantum computing regimes. Unfortunately, non-variational approaches for calculating the spin-adapted ground state naively require $O(n_{\text{spin}}^4)$ quantum gates and are therefore expected to be more resource-intensive. Two straightforward methods are commonly employed in non-variational approaches: preparing spin-adapted initial states and adding penalty terms to the Hamiltonian [27, 37–39]. In the first approach, if an initial state satisfying the desired values of \hat{S}^2 and \hat{S}_z is prepared, the time evolution under a non-variational method that preserves these symmetries can

* takumi.kobori@phys.s.u-tokyo.ac.jp

ideally lead to the desired spin-adapted state. Although this approach is conceptually ideal, practical implementations face significant challenges. Various sources of errors, such as quantum hardware imperfections and algorithmic approximations (e.g., Suzuki-Trotter decompositions [40–45] or Solovay-Kitaev decompositions [3, 46]) can cause deviations from the intended Hilbert subspace. These deviations may lead to the accumulation and amplification of errors during the computation. Therefore, in practical applications, it is crucial to enhance the energy alignment of the solution with the desired spin sector by introducing penalty terms. However, unlike variational approaches, naively introducing a penalty Hamiltonian involving spin operators in non-variational methods is computationally inefficient. Representing penalty terms proportional to $(\hat{S}^2 - s^*(s^* + 1))^2$ typically requires Hamiltonian-dependent unitary operations, such as $e^{-i\mathcal{H}t}$ in ATE, which in turn demand $O(n_{\text{spin}}^4)$ gates. Thus, accelerating the non-variational approaches for obtaining spin-adapted ground states remains a key challenge and an important objective for the realization of fault-tolerant quantum computing in the future.

In this paper, we propose a novel procedure to reduce the computational cost of penalty terms in non-variational methods for spin-rotationally symmetric Hamiltonians. Our method consists of two main steps: the first involves preparing a spin-magnitude-adapted ground state, which is the lowest energy with the desired total spin magnitude, and the second performs post-processing to adjust the spin- z component. In the first step, we introduce an extended penalty term to prepare the spin-magnitude-adapted ground state that adds an additional penalty term related to the spin- z component to the penalty term associated with the total spin magnitude. This modification allows us to eliminate the squared form of the original penalty term and reduce the number of terms from $O(n_{\text{spin}}^4)$ to $O(n_{\text{spin}}^2)$. In the second step, we introduce a post-processing method to obtain the desired S_z states from the spin-magnitude-adapted state. The post-processing can be performed using a quantum circuit with a depth scaling of $O(\log^2 n)$. Typically, in physical systems, the terms of the Hamiltonian are smaller than $O(n_{\text{spin}}^2)$, which means that the square-root reduction in complexity achieved by our method offers significant speedup. To demonstrate the effectiveness of our proposed method, we performed numerical simulations on the Heisenberg ring model and the manganese trimer using ATE and PITE. The successful results demonstrate the versatility of our method.

II. BACKGROUND

A. Non-variational approaches to prepare ground states

Currently, various studies are actively underway worldwide to efficiently calculate ground states on quantum

computers. In this study, we have adopted and compared two ground state calculation methods based on non-variational methods: imaginary time evolution (ITE) method and adiabatic time evolution (ATE) method. This section briefly introduces these methods and discusses the challenges in calculating the spin-adapted ground states using non-variational methods.

1. ATE

ATE is a non-variational method that applies the adiabatic theorem to obtain the ground state of a target Hamiltonian [14, 27, 36]. The adiabatic theorem states that if a system is initially in the ground state of the Hamiltonian and the Hamiltonian evolves sufficiently slowly, the system will remain in the instantaneous ground state throughout the evolution. To prepare the ground state of a Hamiltonian $\mathcal{H}_{\text{problem}}$ using ATE method, the procedure begins by preparing the ground state $|\psi(0)\rangle$ of an initial Hamiltonian $\mathcal{H}_{\text{initial}}$. The system is then evolved under a time-dependent Hamiltonian of the form $\mathcal{H}(t) = (1 - \frac{t}{T})\mathcal{H}_{\text{initial}} + \frac{t}{T}\mathcal{H}_{\text{problem}}$ from $t = 0$ to $t = T$, such that the adiabatic condition is satisfied. The evolution is typically implemented using discrete time steps, applying unitary operators of the form $e^{-i\mathcal{H}(t)\Delta t} |\psi(t)\rangle$. The quantum circuit of ATE is illustrated in Fig. 1(a).

The procedure of ATE is as follows.

Procedure 1 Adiabatic Time Evolution (ATE)

Input: Problem Hamiltonian $\mathcal{H}_{\text{problem}}$, Initial Hamiltonian $\mathcal{H}_{\text{initial}}$, Total evolution time T , Total time step n , Time schedule Δt_i

Output: Ground state of $\mathcal{H}_{\text{problem}}$

- 1: Initialize the state vector $|\psi\rangle$ as the ground state of $\mathcal{H}_{\text{initial}}$
 - 2: $t \leftarrow 0$
 - 3: **for** $i = 0$ to n
 - 4: $\mathcal{H}_t \leftarrow (1 - \frac{t}{T})\mathcal{H}_{\text{initial}} + \frac{t}{T}\mathcal{H}_{\text{problem}}$
 - 5: $|\psi\rangle \leftarrow e^{-i\mathcal{H}_t\Delta t_i} |\psi\rangle$
 - 6: $t \leftarrow t + \Delta t_i$
 - 7: **return** $|\psi\rangle$
-

Several factors must be taken into account when implementing ATE. First, the total evolution time T is typically large, and the time steps Δt_i must be sufficiently small, making ATE computationally demanding. The values of T and Δt_i are closely related to the energy gap between the ground state and the first excited state of the system. Consequently, selecting an appropriate initial Hamiltonian $\mathcal{H}_{\text{initial}}$ that maintains a sufficiently large energy gap throughout the evolution is crucial. Second, there exists a systematic error associated with the implementation of the time evolution operator $e^{-i\mathcal{H}(t)\Delta t}$ on a quantum circuit. This operation is typically achieved using the Suzuki-Trotter decomposition, which introduces decomposition errors. These decomposition errors must be carefully considered.

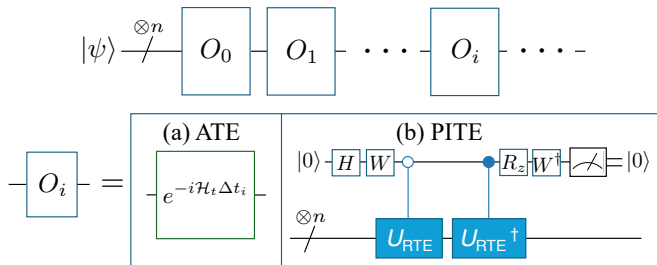


FIG. 1: Circuits of the non-variational approaches: (a) ATE and (b) PITE. In (b), $U_{\text{RTE}} = e^{-i\mathcal{H}s\Delta t}$.

2. ITE and probabilistic ITE (PITE)

ITE is a non-variational method that applies the imaginary-time evolution of a Hamiltonian to obtain the ground state. The state $|\psi(\tau)\rangle$ after evolving an initial state $|\psi(0)\rangle$ for an imaginary time τ is given by

$$\begin{aligned} |\psi(\tau)\rangle &\propto e^{-\mathcal{H}\tau} |\psi(0)\rangle \\ &\propto \sum_{E_i} e^{-E_i\tau} |\psi_i\rangle \langle \psi_i | \psi(0)\rangle, \end{aligned} \quad (1)$$

where $|\psi_i\rangle$ and E_i are the eigenstates and corresponding eigenvalues of the Hamiltonian \mathcal{H} , respectively. Because the exponential factor $e^{-E_i\tau}$ suppresses contributions from excited states according to their energy, the amplitude of the excited states decays exponentially with increasing τ . Therefore, evolution for a sufficiently long imaginary time effectively projects the system onto the ground state. ITE has been widely employed in classical simulations of quantum systems [47, 48]. However, the imaginary time evolution operator $e^{-\mathcal{H}\tau}$ is non-unitary, and its implementation on a quantum computer is non-trivial. Several approaches to realize ITE on a quantum computer [15, 16, 21, 49–53] have been proposed. In this work, we focus on the probabilistic imaginary time evolution (PITE) method [18, 33–35].

PITE is a method to realize ITE on a quantum computer by using ancilla qubits, measurements, and post-selection. While several implementations of PITE have been proposed, in this work we adopted the method proposed by Kosugi *et al.* [18]. Compared with other PITE approaches, the method by Kosugi offers notable advantages: it requires only a single ancilla qubit and minimal classical post-processing. These features make it particularly suitable for an early fault-tolerant quantum computing algorithm.

To implement the non-unitary operator $\mathcal{M} = m_0 e^{-\mathcal{H}\tau}$ for imaginary time evolution, where m_0 is an adjustable constant satisfying $0 < m_0 < 1$ and $m_0 \neq 1/\sqrt{2}$, we extend the n -qubit system $|\psi\rangle$ to an $(n+1)$ -qubit system by introducing an ancilla qubit. The unitary operation

$U_{\mathcal{M}}$ is defined as

$$U_{\mathcal{M}}(|0\rangle \otimes |\psi\rangle) = |0\rangle \otimes \mathcal{M}|\psi\rangle + |1\rangle \otimes \sqrt{1 - \mathcal{M}^2}|\psi\rangle. \quad (2)$$

This operation can be realized by the following $2^{n+1} \times 2^{n+1}$ unitary operation

$$U_{\mathcal{M}} = \begin{pmatrix} \mathcal{M} & \sqrt{1 - \mathcal{M}^2} \\ -\sqrt{1 - \mathcal{M}^2} & \mathcal{M} \end{pmatrix}. \quad (3)$$

By using this unitary operation $U_{\mathcal{M}}$, the non-unitary operator \mathcal{M} can be realized by initializing the ancilla qubit to $|0\rangle$, applying $U_{\mathcal{M}}$ and post-selecting the measurement outcome of the ancilla qubit to be $|0\rangle$. $U_{\mathcal{M}}$ can be decomposed as

$$U_{\mathcal{M}} = (W^\dagger \otimes I) \begin{pmatrix} e^{i\kappa\Theta} & 0 \\ 0 & e^{-i\kappa\Theta} \end{pmatrix} (WH \otimes I), \quad (4)$$

where H is the Hadamard gate, W and Θ are described below,

$$W = \frac{1}{\sqrt{2}} \begin{pmatrix} 1 & -i \\ 1 & i \end{pmatrix}, \quad \Theta = \arccos \frac{\mathcal{M} + \sqrt{1 - \mathcal{M}^2}}{\sqrt{2}}, \quad (5)$$

and κ is a constant given by $\kappa = \text{sgn}(m_0 - 1/\sqrt{2})$. The central component of $U_{\mathcal{M}}$ can be implemented using controlled unitaries $e^{\pm i\kappa\Theta}$.

Although the above methods are non-approximate, the computational cost of preparing controlled unitaries $e^{\pm i\kappa\Theta}$ is typically high. Therefore, in practice, these controlled unitaries are approximated in the first-order Taylor expansion of the imaginary time. To account for the approximation, we expand $\kappa\Theta$ using a Taylor series as $\kappa\Theta = \theta_0 - \mathcal{H}s\Delta t + O(\Delta t^2)$, where $\theta_0 = \kappa \arccos[(m_0 + \sqrt{1 - m_0^2})/\sqrt{2}]$ and $s = m_0/\sqrt{1 - m_0^2}$. By utilizing such an approximation, Eq. (4) can be rewritten as

$$U_{\mathcal{M}} = (W^\dagger R_z(-2\theta_0) \otimes I) \begin{pmatrix} e^{-i\mathcal{H}s\Delta t} & 0 \\ 0 & e^{i\mathcal{H}s\Delta t} \end{pmatrix} (WH \otimes I) + O(\Delta t^2), \quad (6)$$

where $R_z(\theta)$ is the rotation operator around the z -axis by an angle θ , defined as $R_z(\theta) = e^{-i\theta\sigma_z/2}$. The controlled unitaries $e^{\pm i\mathcal{H}s\Delta t}$ can be implemented via the real-time evolution of the Hamiltonian \mathcal{H} as illustrated in Fig. 1(b), enabling practical implementation. The overall procedure of PITE is summarized as follows:

Procedure 2 Probabilistic Imaginary Time Evolution (PITE)

Input: Problem Hamiltonian $\mathcal{H}_{\text{problem}}$, Initial state $|\psi\rangle_0$, Total steps N , Time step Δt , Coefficient m_0

Output: Ground state of $\mathcal{H}_{\text{problem}}$

- 1: $s \leftarrow m_0/\sqrt{1-m_0^2}$
 - 2: $\kappa \leftarrow \text{sgn}(m_0 - 1/\sqrt{2})$
 - 3: $\theta_0 \leftarrow \kappa \arccos \left[(m_0 + \sqrt{1-m_0^2})/\sqrt{2} \right]$
 - 4: $|\psi\rangle \leftarrow |\psi\rangle_0$
 - 5: **for** $t = 0$ to N
 - 6: Add ancilla qubit $|0\rangle$: $|\psi\rangle \leftarrow |0\rangle \otimes |\psi\rangle$
 - 7: Apply the circuit as shown in Fig. 1(b):
 - 8: $|\psi\rangle \leftarrow (WH \otimes I) |\psi\rangle$
 - 9: $|\psi\rangle \leftarrow (|0\rangle\langle 0| \otimes e^{-i\mathcal{H}_S \Delta t} + |1\rangle\langle 1| \otimes I) |\psi\rangle$
 - 10: $|\psi\rangle \leftarrow (|0\rangle\langle 0| \otimes I + |1\rangle\langle 1| \otimes e^{i\mathcal{H}_S \Delta t}) |\psi\rangle$
 - 11: $|\psi\rangle \leftarrow (W^\dagger R_z(-2\theta_0) \otimes I) |\psi\rangle$
 - 12: Measure the ancilla qubit and post-select to $|0\rangle$:
 - 13: $|\psi\rangle \leftarrow (|0\rangle\langle 0| \otimes I) |\psi\rangle$
 - 14: **return** $|\psi\rangle$
-

Like ATE, the time schedule of PITE can be adjustable, but in our numerical experiments, Δt is set to a constant. Similarly, m_0 is typically fixed throughout the evolution. However, if the lowest eigenvalue of $\mathcal{H}_{\text{problem}}$ are known in advance, m_0 can be optimized accordingly to improve performance [17, 54].

B. Difficulty of non-variational approach for spin-adapted ground states

The simplest way to obtain the spin-adapted ground state is to add penalty terms of the spin operators to the original Hamiltonian. However, since expectation values of physical observables cannot be measured during the execution of non-variational algorithms, it is not possible to use the same penalty terms as in variational methods. The penalty terms for non-variational methods are based on the total spin magnitude $\hat{S} = \sum_{i=0}^{n_{\text{spin}}-1} \sigma_i/2$ and the z -component spin operator $\hat{S}_z = \sum_{i=0}^{n_{\text{spin}}-1} \sigma_{iz}/2$ as

$$\begin{aligned} \mathcal{H}_{\text{penalty}} &= C_S (\hat{S}^2 - s^*(s^* + 1))^2 + C_z (\hat{S}_z - s_z^*)^2 \\ &\equiv C_S \mathcal{H}_S + C_z \mathcal{H}_z, \end{aligned} \quad (7)$$

where n_{spin} is the number of spins, $\sigma_{i\mu}$ are the Pauli μ matrices acting on i -th spin (μ is x , y , or z), C_s and C_z are positive constants. The parameters s^* and s_z^* are the target total spin magnitude and z -component, respectively. By adding the penalty terms to the original Hamiltonian, the resulting ground state will satisfy the desired spin properties.

Here we discuss the number of terms involved in the penalty terms. In particular, we compare the number of terms between \mathcal{H}_S and \mathcal{H}_z . \mathcal{H}_z has fewer terms than \mathcal{H}_S because of the squared form of \hat{S}^2 in \mathcal{H}_S . To discuss the \mathcal{H}_S penalty term in more detail, we consider the term

$\sigma_i \cdot \sigma_j$. If $i = j$, we have $\sigma_i \cdot \sigma_i = \sigma_i^2 = 3I$. For $i \neq j$,

$$\begin{aligned} \sigma_i \cdot \sigma_j |00\rangle_{ij} &= |00\rangle_{ij} \\ \sigma_i \cdot \sigma_j |01\rangle_{ij} &= 2|10\rangle_{ij} - |01\rangle_{ij} \\ \sigma_i \cdot \sigma_j |10\rangle_{ij} &= 2|01\rangle_{ij} - |10\rangle_{ij} \\ \sigma_i \cdot \sigma_j |11\rangle_{ij} &= |11\rangle_{ij}. \end{aligned} \quad (8)$$

By using the swap matrices U_{ij}^S that exchanges spin i and spin j , the term $\sigma_i \cdot \sigma_j$ can be expressed as

$$\sigma_i \cdot \sigma_j = 2U_{ij}^S - I. \quad (9)$$

Using the above relation, the \hat{S}^2 term can be rewritten as

$$\hat{S}^2 = \frac{n_{\text{spin}}(4 - n_{\text{spin}})}{4} + \sum_{i>j} U_{ij}^S. \quad (10)$$

It indicates that in the variational method, performing at least $O(n_{\text{spin}}^2)$ measurements is sufficient to evaluate the penalty term [55]. Moreover, depending on the encoding method, it is possible to evaluate multiple $\langle U_{ij}^S \rangle$ terms using a single circuit. For example, in a naive encoding where each spin is assigned to a distinct qubit, the penalty term can be evaluated using only $O(n_{\text{spin}})$ different circuits.

The \mathcal{H}_S penalty term can be expressed by U_{ij}^S as

$$\begin{aligned} \mathcal{H}_S &= (\hat{S}^2 - s^*(s^* + 1))^2 \\ &= a^2 - 2a \sum_{i>j} U_{ij}^S + \left(\sum_{i>j} U_{ij}^S \right)^2, \end{aligned} \quad (11)$$

where $a = n_{\text{spin}}(4 - n_{\text{spin}})/4 - s^*(s^* + 1)$ [56]. The last term involves all pairwise products of swap operators, resulting in a total of $O(n_{\text{spin}}^4)$ terms. Consequently, evaluating \mathcal{H}_S in non-variational methods leads to a worst-case computational complexity of $O(n_{\text{spin}}^4)$, whereas variational methods require only $O(n_{\text{spin}}^2)$ [29, 57]. This reduction highlights the practical advantage of variational approaches in preparing spin-adapted states. While non-variational methods can achieve some degree of reduction by parallelizing the evaluation of the U_{ij}^S terms, for example in the case of PITE, this can be achieved by increasing the number of ancilla qubits [58], such parallelization can also be incorporated into variational methods, and the overall time complexity remains less favorable than those of variational methods. This underscores the need for the development of more fundamental approaches to reduce the computational cost in non-variational approaches further.

III. METHOD

In this section, we propose a novel method to address the issue mentioned above in spin-adapted state prepa-

ration when the original system Hamiltonians have spin-rotational symmetry. Our approach enables a square-root reduction in the number of terms required for the penalty term. Our proposed method is based on the following two main steps:

1. Prepare the spin-magnitude-adapted ground state with maximal spin- z component (i.e. $S_z = s^*$) using a non-variational method.
2. Apply a rotation operator within the subspace that conserves the total spin, followed by a projection onto the subspace corresponding to a desired Hamming weight of given S_z .

By introducing the two-step procedure as described above and obtaining the ground state for the Hamiltonian with the properly constructed penalty terms using non-variational approaches, we successfully reduce the number of terms in the penalty Hamiltonian from $O(n_{\text{spin}}^4)$ to $O(n_{\text{spin}}^2)$, thereby achieving a quadratic speedup. It is worth noting that the proposed method is expected to have broad applicability since many Hamiltonians exhibit spin-rotational symmetry [59–62].

A. Prepare the spin-magnitude-adapted ground state with maximal S_z

By restricting the target ground state to the subspace of $S_z = s^*$, we can reduce the number of terms in the penalty Hamiltonian for the total spin magnitude to $O(n_{\text{spin}}^2)$. The penalty term can be written as

$$\mathcal{H}'_{\text{penalty}} = C_S(\hat{S}^2 - s^*(s^* + 1)) - C_z(\hat{S}_z - s^*) \quad (12)$$

$$\equiv C_S \mathcal{H}'_S + C_z \mathcal{H}'_z. \quad (13)$$

By eliminating the quadratic terms, we successfully reduce the number of terms from $O(n_{\text{spin}}^4)$ to $O(n_{\text{spin}}^2)$. The eigenvalues of this modified penalty Hamiltonian for the spin eigenfunctions $|s, s_z\rangle$ are given by

$$\begin{aligned} E_{\text{penalty}}(s, s_z) &\equiv \langle s, s_z | (C_S \mathcal{H}'_S + C_z \mathcal{H}'_z) | s, s_z \rangle \\ &= C_S (s(s+1) - s^*(s^*+1)) - C_z (s_z - s^*). \end{aligned} \quad (14)$$

The minimum eigenvalue with respect to s_z for a given s is obtained at $s_z = s$:

$$\begin{aligned} E_{\text{penalty}}(s) &\equiv \min_{s_z} E_{\text{penalty}}(s, s_z) \\ &= E_{\text{penalty}}(s, s) \\ &= C_S (s(s+1) - s^*(s^*+1)) - C_z (s - s^*). \end{aligned} \quad (15)$$

Since this is a quadratic function of s , to attain the minimum value at $s = s^*$, it must satisfy the inequality $E_{\text{penalty}}(s^* - 1) > E_{\text{penalty}}(s^*)$ and $E_{\text{penalty}}(s^*) <$

$E_{\text{penalty}}(s^* + 1)$. Therefore, the condition for the minimum eigenvalue of the penalty Hamiltonian is given by

$$2s^* < \frac{C_z}{C_S} < 2(s^* + 1). \quad (16)$$

Under this condition, the spin-adapted ground state with maximal S_z can be efficiently prepared by non-variational methods. Also, the ground state with minimal S_z , i.e., $S_z = -s^*$, can be obtained by the similar procedure. It should be noted that the coefficients C_S and C_z must be chosen sufficiently large to prevent contamination from other undesired spin states. Although the above discussion focuses solely on the penalty terms, the total Hamiltonian can be written as $\mathcal{H}_{\text{problem}} = \mathcal{H}_{\text{system}} + \mathcal{H}_{\text{penalty}}$, where $\mathcal{H}_{\text{system}}$ is the original system Hamiltonian. If the penalty coefficients are too small, the resulting ground state of the total Hamiltonian may not correspond to the desired total spin magnitude. Therefore, the coefficients must be set large enough so that the terms $\mathcal{H}_{\text{penalty}}$ are dominant. On the other hand, excessively large coefficients may require a smaller time step Δt in the non-variational evolution, leading to a decrease in the computational efficiency. Hence, the penalty strengths must be appropriately optimized for each specific system.

B. Post processing to achieve the desired S_z

Post processing lies in a projection operator to vary S_z onto the desired S_z state while maintaining the total spin magnitude. Such a projection operation can be implemented using a rotation operator within the spin- S subspace. Here, we consider the rotation operator around the y -axis defined as $U_y(\theta) = e^{-i\theta\hat{S}_y}$, where $\hat{S}_y = \sum_i \sigma_{iy}/2$. Due to the additive structure of \hat{S}_y , the rotation operator can be implemented by the depth-1 circuit as $U_y(\theta) = e^{-i\theta\sigma_y/2} \otimes \dots \otimes e^{-i\theta\sigma_y/2}$. Importantly, due to the spin-rotational symmetry of the Hamiltonian, the rotated state remains within the desired ground state corresponding to the total spin magnitude $S = s^*$. This allows us to explore different S_z states while ensuring that the system remains in the desired spin subspace.

The remaining task is to determine the optimal rotation angle θ corresponding to the desired s_z^* . For later projection onto the target s_z^* eigenstate from the obtained state $|s^*, s_z = s^*\rangle$, it is necessary to maximize the probability of obtaining the desired S_z state. The weight of the target state in the rotated state is given as

$$w_c(\theta) \equiv \left| d_{s_z^* s^*}^{s^*}(\theta) \right|^2 = \left| \langle s^*, s_z^* | e^{-i\theta\hat{S}_y} | s^*, s^* \rangle \right|^2, \quad (17)$$

where $d_{s_z^* s^*}^{s^*}$ is the Wigner D-matrix element [63]. It can be expressed as

$$d_{s_z^* s^*}^{s^*}(\theta) = \sqrt{\frac{(2s^*)!}{(s^* + s_z^*)!(s^* - s_z^*)!}} \left(\cos \frac{\theta}{2} \right)^{s^* + s_z^*} \left(\sin \frac{\theta}{2} \right)^{s^* - s_z^*}. \quad (18)$$

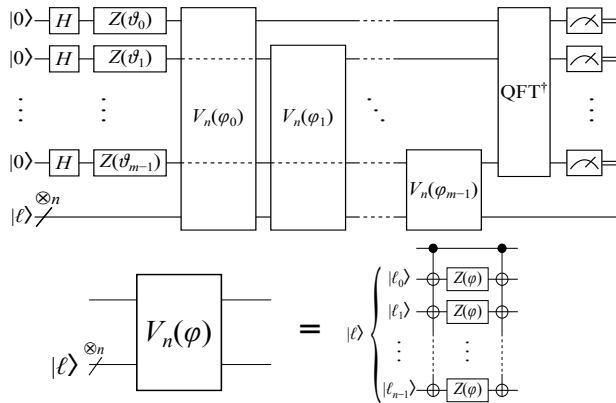


FIG. 2: Circuit for projecting an n -qubit input $|l\rangle$ onto the subspace with a specified Hamming weight, using $m = \lceil \log_2 n \rceil$ ancilla qubits. The circuit parameters are given by $\vartheta_k = 2^{k-m}\pi n$ and $\varphi_k = -2^{k-m}\pi$ [64]. Post-selection on the measurement outcomes of the ancilla qubits ensures the correct projection.

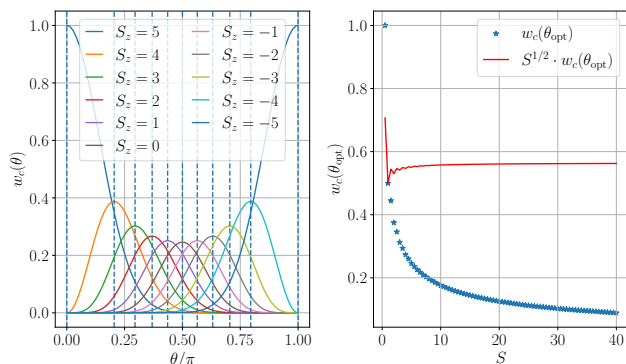


FIG. 3: (Left) θ -dependence of the weight of the various S_z states for $S = 5$. Each line represents a different S_z and each vertical dotted line represents θ_{opt} . (Right) Dependency of minimum $w_c(\theta_{\text{opt}})$ in S_z on S . S_z are set to $S_z = 0$ or $S_z = 1/2$.

Thus, the optimal θ for the maximum $d_{s_z^*}^{s_z^*}$ is given by

$$\theta_{\text{opt}} = 2 \arcsin \sqrt{\frac{s^* - s_z^*}{2s^*}}. \quad (19)$$

The optimality of this value is also supported by the numerical results shown in Fig. 3 (Left). The weight of obtaining the desired S_z state is given by

$$w_c(\theta_{\text{opt}}) = \frac{(2s^*)!}{(s^* + s_z^*)!(s^* - s_z^*)!} \frac{(s^* + s_z^*)^{s^* + s_z^*} (s^* - s_z^*)^{s^* - s_z^*}}{(2s^*)^{2s^*}}. \quad (20)$$

The second operation is the projection onto the desired S_z state. In general, the S_z eigenstates can be described

in terms of the computational basis states $|j\rangle$. Specifically, if n_1 denotes the number of ones in the binary representation of j , the corresponding S_z eigenstate is given by $|j\rangle$ where $n_1 = n_{\text{spin}}/2 - S_z$. Thus, the projection operation can be realized by projection onto the subspace with Hamming weight $n_{\text{spin}}/2 - S_z$, as illustrated in Fig. 2. The depth of the circuit implementing this projection is $O(\log^2 n)$. To analyze the success probability of post-selection, we plotted the dependency of the minimum $w_c(\theta_{\text{opt}})$ across S_z on given S , which characterizes the minimum success probability of post-selection, in Fig. 3. The results indicate that the success probability scales as $O(S^{-1/2})$. The behavior can also be derived from the properties of Catalan numbers [65]. In condensed matter physics, obtaining low- S spin-adapted states is often of primary importance, implying that small S values are sufficient in practice. Thus, the present procedure is more efficient than the first step of our approach described in Sec. III A. It should be noted that for binary encoding [66], as shown in Appendix A and used, for instance, in the calculation of the manganese trimer, a modification of the circuit is necessary. With binary encoding, a d -level system can be represented by $O(\log d)$ qubits. However, the depth of the unitary operation may increase exponentially in the worst case, as such encodings generally sacrifice the simple expressivity of quantum gates [67]. Nonetheless, in condensed matter physics, d of each spin or molecule is typically small, and the resulting overhead is not practically significant.

IV. NUMERICAL EXPERIMENTS

In the following numerical experiments, we focus on evaluating the performance of the first step. Accordingly, throughout this section, the desired spin- z s_z^* is set to s^* .

A. Spin-1/2 Heidenberg ring model

In this numerical experiment, we consider the spin-1/2 Heidenberg ring model [69]. Its Hamiltonian is given by

$$\mathcal{H}_{\text{system}} = \sum_{i=0}^{n_{\text{spin}}-1} 2J_i \hat{S}_i \cdot \hat{S}_{i+1} = \frac{1}{2} \sum_{i=0}^{n_{\text{spin}}-1} J_i \sigma_i \cdot \sigma_{i+1},$$

where the periodic boundary condition is assumed and $\sigma_{n_{\text{spin}}} = \sigma_0$. In this numerical experiment, J_i is fixed to $J_i = 2$.

The results of $n_{\text{spin}} = 6$ are shown in Fig. 4 for ATE and Fig. 5 for PITE. In Fig. 4, parameters are $T = 1.0$, $n = 2 \times 10^4$, $C_S = 10$ and $C_z = C_S(2s^* + 1)$. The time schedule of Δt_i is defined by a sine function as $\Delta t_i = \sin^2(2\pi t) \times 10^{-4}$. The initial Hamiltonian is like $\mathcal{H}_{\text{initial}} = \sum_i (-1)^i \sigma_{ix}$ and its initial states are ones in which plus states $|+\rangle$ and minus states $|-\rangle$ are arranged alternately. In Fig. 5, we evaluate the convergence by comparing our proposed penalty terms with the conventional penalty

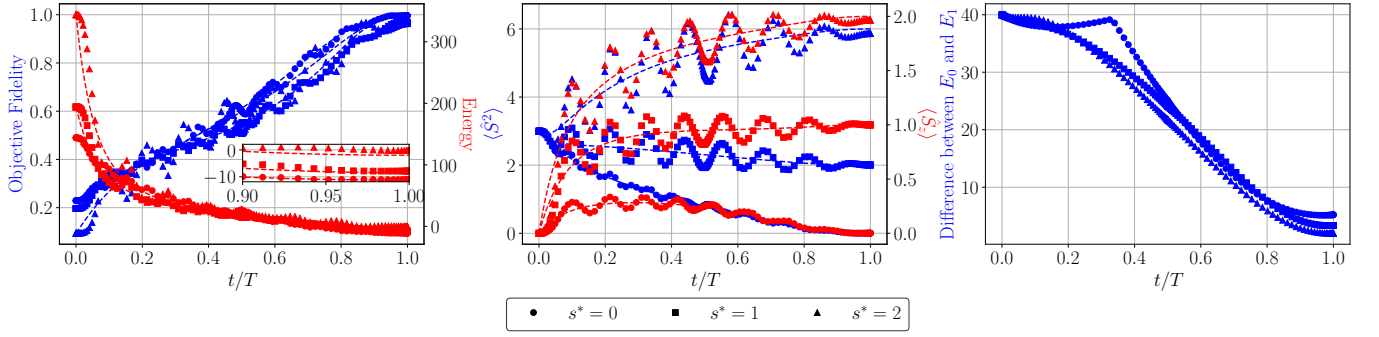


FIG. 4: Results of our proposed methods for preparing spin-adapted ground states of Heisenberg ring models by ATE. Different markers represent the target spin quantum numbers s^* : circles, squares, and rectangles correspond to $s^* = 0$, $s^* = 1$, and $s^* = 2$, respectively. The vertical axes represent various physical observables. “Objective Fidelity” (blue) denotes the fidelity between the target state and the instantaneous state. “Energy” (red), “ $\langle \hat{S}^2 \rangle$ ” (blue), and “ $\langle \hat{S}_z \rangle$ ” (red) represent the expectation values of $\mathcal{H}_{\text{problem}}$, \hat{S}^2 , and \hat{S}_z , respectively. The dotted lines in each panel represent the exact values of the corresponding observables, obtained via exact diagonalization of the instantaneous Hamiltonian \mathcal{H}_t .

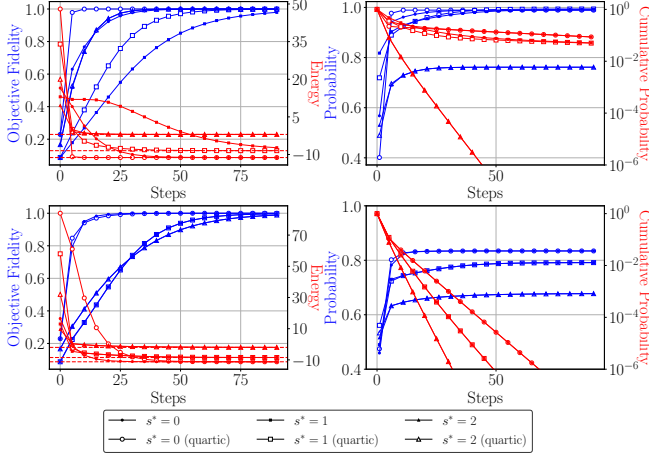


FIG. 5: Results comparing our proposed method with conventional penalty approach (quartic) in PITE. The top two figures show results of $\Delta t = 0.05$, with $C_S = 7.5$ for our method (filled markers) and $C_S = 3$ for the conventional method (open markers), while the bottom two figures show results of $\Delta t = 0.015$ with $C_S = 7.5$ for our method, and $C_S = 5$ for the conventional method. “Probability” indicates the success probability of post-selection at each step, while “Cumulative Probability” denotes the accumulated success probability up to a given step. The dotted lines represent the exact values of $\mathcal{H}_{\text{problem}}$.

term (Eq. 7) under two different parameter settings for C_S , and Δt (see caption). The common parameters are $m_0 = 0.8$ and $C_z = C_S(2s^* + 1)$. The initial states for the PITE simulations are $|\psi\rangle_0 = \bigotimes_{i=0}^{s^*+2} |0\rangle \bigotimes_{i=s^*+3}^{n_{\text{spin}}-1} |1\rangle$. s^*_z quantum numbers of the initial states are already set to the desired values s^* to focus on the dependence of

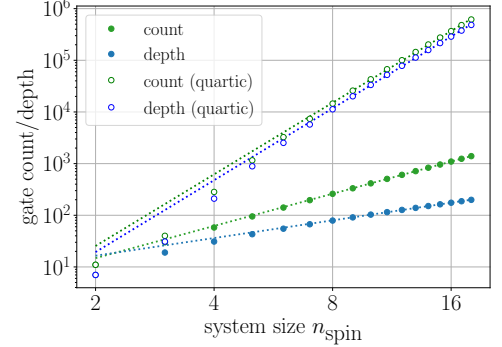


FIG. 6: Dependence of gate complexity of penalty terms for spin magnitude on the system size n_{spin} . The plots were calculated by transpiling the time evolution operators, $\exp(-iC_S\mathcal{H}_S^{(l)}s\Delta t) = \exp(-0.15i\mathcal{H}_S^{(l)})$, where $C_S = 7.5$, $\Delta t = 0.015$, and $m_0 = 0.8$, into a gate set consisting of arbitrary single-qubit unitaries and CNOT gates. The transpilation was performed using the transpile function from Qiskit [68]. Data points with $n_{\text{spin}} \geq 8$ were fitted to power laws, and the fitted curves are shown as dotted lines. The fitting results are count: $y = 3.53n_{\text{spin}}^{2.07}$, depth: $y = 7.51n_{\text{spin}}^{1.14}$, count (quartic): $y = 1.04n_{\text{spin}}^{4.61}$, and depth (quartic): $y = 0.79n_{\text{spin}}^{4.62}$.

the spin-magnitude penalty, and they remain unchanged during the PITE calculations.

The figures in Fig. 4 demonstrate that the results of ATE successfully track the dotted lines, which represent the exact evolution based on the diagonalization of the instantaneous Hamiltonian \mathcal{H}_t . In general, hyperparameters such as the time schedule Δt_i , C_S , and C_z influence performance. Δt should be chosen to be sufficiently small to ensure accuracy, whereas C_S and C_z should be

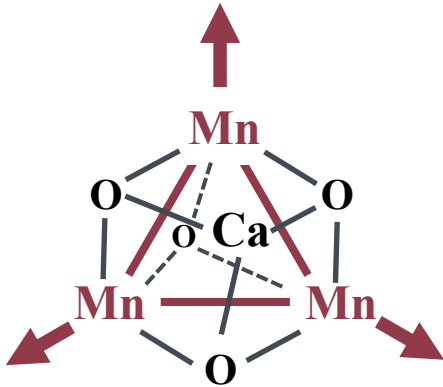


FIG. 7: Schematic of a cubane-like CaMn_3O_4 cluster.

taken sufficiently large to avoid significant fidelity loss. Focusing on the deviation from the ideal energy value, the deviation increases in the order of $s^* = 0$, $s^* = 1$, and $s^* = 2$. Although there is some dependence on the initial state, achieving accurate outcomes with ATE becomes increasingly challenging as the excitation level increases. The excitation level is determined by the energy gap between the ground state E_0 and the first excited state E_1 of the instantaneous Hamiltonian \mathcal{H}_t , as shown in the right panel of Fig. 4. Oscillatory behavior is also observed in the results. It comes from the approximation of an infinite-time schedule by a finite-time one. In fact, similar oscillations have been reported for penalty Hamiltonians for spin magnitude [27]. These oscillations depend on the derivative of the time schedule at $t = 0$ and $t = T$, and they occur when these derivatives are nonzero. The derivative of the time schedule in this numerical experiment becomes non-zero in the third order, which is consistent with the best-performing schedules identified by Hu *et al.* [70]. This suggests that our proposed method may be inherently prone to oscillatory trajectories.

The results presented in Fig. 5 demonstrate that the PITE calculations successfully converge toward the reference values denoted by the dotted lines. In the upper two panels, the conventional penalty method (quartic) exhibits a faster convergence rate compared to our proposed method, whereas the lower panels show comparable convergence behavior between the two methods. This indicates that the convergence properties depend on other parameters, problem settings, and the characteristics of the target states. Conversely, when examining the gate complexity in Fig. 6, a clear and consistent gap is observed between the two penalty approaches. The dependencies in Fig. 6 align well with the rough complexity estimates discussed in previous sections. Generally, it can be stated that in PITE, the cumulative success probability decreases exponentially with the increasing number of steps. Therefore, selecting an appropriate number of steps based on the target success probability is essen-

tial for practical applications. The success probability at each step depends on the instantaneous quantum states; thus, preparing an initial state close to the desired state, such as by performing ATE before the PITE steps, is crucial. The success probabilities observed for our proposed method in the numerical experiments are comparable to those of the conventional approach and remain reasonably high in several cases, indicating that our method is practically feasible within the considered problem settings.

B. Manganese Trimer

The oxygen in the atmosphere is known to be generated via the oxidation process of water that occurs at the oxygen-evolving center (OEC) site within photosynthesis system II (PSII) [71]. The experimental results indicate the existence of a manganese cluster in the OEC. The possible geometries of the cluster and their electronic structure, including spin states, are important for elucidating the mechanism of photosynthesis (see Refs. [72, 73] and references therein). Let us consider here a spin trimer that models the spin states of the central part, CaMn_3O_4 of the Mn cluster [See Fig. 7]. The proposed scheme in the present study is applicable to spins whose magnitudes are other than $1/2$, as will be demonstrated below.

The Heisenberg Hamiltonian for the spin trimer reads

$$\mathcal{H}_{\text{system}} = -2J_{01}\hat{S}_0 \cdot \hat{S}_1 - 2J_{12}\hat{S}_1 \cdot \hat{S}_2 - 2J_{20}\hat{S}_2 \cdot \hat{S}_0, \quad (21)$$

where \hat{S}_i represents the spin operator for a manganese ion, and J_{ij} is the coefficient to represent the effective exchange interactions. In this calculation, we explore (II, II, III) set of valences in manganese. The spin magnitudes of Mn(II) and Mn(III) are $S = 5/2$ and $S = 2$ respectively and J_{ij} values of Mn(II)-Mn(II) and Mn(II)-Mn(III) are -1 and -50 (cm^{-1}) respectively [73].

In these numerical experiments, we try to obtain the $s^* = 2$, $s^* = 3$, and $s^* = 4$ spin-adapted ground states. In these models, ones of $s^* = 3$ are ground states and ones of $s^* = 2$ are first excited states. The results are shown in Fig. 8. In Fig. 8 for ATE, the parameters are $T = 1.0$, $n = 2 \times 10^4$, $C_S = 3$ and $C_z = C_S(2s^* + 1)$. The time schedule is the same as one of ATE for the Heisenberg Hamiltonian. In Fig. 8 for PITE, parameters are $\Delta t = 0.008$, and $m_0 = 0.8$. C_S and C_z are the same as those of ATE. For simulating the quantum system of $S = 2$ and $S = 5/2$, the spin state should be encoded in qubit systems. Here, we encoded them by standard binary encoding as shown in Appendix A. For the binary encoding, representing $S = 2$ and $S = 5/2$ states requires three qubits. We set initial states to the computational basis like $|000\rangle \otimes |000\rangle \otimes |100\rangle$ for $s^* = 2$, $|000\rangle \otimes |001\rangle \otimes |100\rangle$ for $s^* = 3$ and $|000\rangle \otimes |000\rangle \otimes |011\rangle$ for $s^* = 4$ where the first and second states represent the encoded states of $S = 5/2$ in Mn(II) and the third

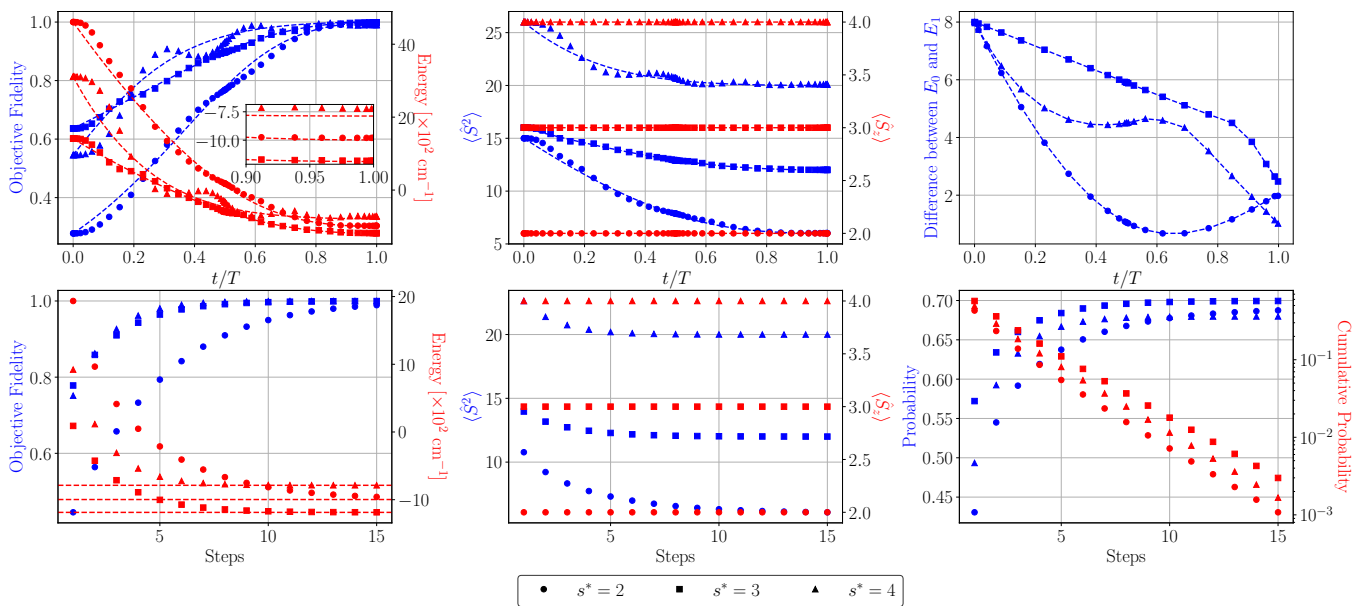


FIG. 8: Results of our proposed methods for preparing spin-adapted ground states of the manganese trimer model. The top three are results of ATE, and the bottom two are results of PITE. The axes, labels, and notation follow the same conventions as used in Fig. 4 and Fig. 5.

states represent ones of $S = 2$ in Mn(III). The same initial states are used for both ATE and PITE. The initial Hamiltonian for ATE is set according to the initial states like $\mathcal{H}_{\text{initial}} = \sum_i (-1)^{f(i)} \sigma_{iz}$ by adjusting the function of $f : \{0, 1, \dots, 8\} \rightarrow \{0, 1\}$. It is worth noting that the initial states are already constrained to the desired values of $\langle \hat{S}_z \rangle$, but not of $\langle \hat{S}^2 \rangle$. Throughout these calculations, only $\langle \hat{S}^2 \rangle$ evolves to attain the correct spin-adapted ground states.

Both the ATE and PITE results shown in Fig. 8 demonstrate successful outcomes, consistent with those obtained for the Heisenberg ring model. By incorporating the proposed penalty terms, the methods can capture not only the ground state but also certain excited states. These findings indicate that our proposed methods are applicable not only to simple spin models but also to more practical and complex systems.

V. SUMMARY AND OUTLOOK

In this work, we have proposed novel methods to reduce the computational cost of penalty terms for obtaining spin-adapted ground states of spin-rotationally symmetric Hamiltonians, from $O(n_{\text{spin}}^4)$ to $O(n_{\text{spin}}^2)$. To describe the practical utilities, we have shown the results for spin-1/2 Heisenberg ring models and the manganese trimer by ATE and PITE. For the manganese trimer,

since there are few reports on the results of ATE and PITE, the novelty of this work also lies in demonstrating the feasibility of these methods for such a system.

Our main method only modifies the penalty term for spin variables, and it is widely applicable. The preparation of excited states is generally more challenging than that of the ground state [74–79]. However, our method enables the preparation of certain specific excited states using the same procedure as ground state preparation. Also, it can be applied not only to various spin systems but also to first-quantized Hamiltonian [18, 36, 80–82]. First-quantized formalism is considered more efficient for calculations in systems with a fixed particle number than second-quantized formalism. In such more complicated systems, the spin degrees of freedom can be treated independently from the spatial degrees of freedom, making them within the scope of our method.

ACKNOWLEDGMENTS

This work was supported by the Center of Innovation for Sustainable Quantum AI, JST Grant Number JPMJPF2221. TK acknowledges the support of JST SPRING, Grant Number JPMJSP2108. The authors thank the Supercomputer Center, the Institute for Solid State Physics, the University of Tokyo, for the use of the facilities.

[1] A. W. Sandvik, in *AIP Conference Proceedings*, Vol. 1297 (American Institute of Physics, 2010) pp. 135–338.

[2] R. P. Feynman, in *Feynman and computation* (cRc

- Press, 2018) pp. 133–153.
- [3] M. A. Nielsen and I. L. Chuang, *Quantum computation and quantum information* (Cambridge university press, 2010).
 - [4] R. Orús, *Nature Reviews Physics* **1**, 538 (2019).
 - [5] I. M. Georgescu, S. Ashhab, and F. Nori, *Rev. Mod. Phys.* **86**, 153 (2014).
 - [6] G. H. Low and I. L. Chuang, *Quantum* **3**, 163 (2019).
 - [7] B. Bauer, S. Bravyi, M. Motta, and G. K.-L. Chan, *Chemical Reviews* **120**, 12685 (2020).
 - [8] M. Cerezo, A. Arrasmith, R. Babbush, S. C. Benjamin, S. Endo, K. Fujii, J. R. McClean, K. Mitarai, X. Yuan, L. Cincio, and P. J. Coles, *Nature Reviews Physics* **3**, 625 (2021).
 - [9] Y. Cao, J. Romero, J. P. Olson, M. Degroote, P. D. Johnson, M. Kieferová, I. D. Kivlichan, T. Menke, B. Peropadre, N. P. D. Sawaya, S. Sim, L. Veis, and A. Aspuru-Guzik, *Chemical Reviews* **119**, 10856 (2019).
 - [10] D. Wu, R. Rossi, F. Vicentini, N. Astrakhantsev, F. Becca, X. Cao, J. Carrasquilla, F. Ferrari, A. Georges, M. Hibat-Allah, M. Imada, A. M. Läuchli, G. Mazzola, A. Mezzacapo, A. Millis, J. Robledo Moreno, T. Neupert, Y. Nomura, J. Nys, O. Parcollet, R. Pohle, I. Romero, M. Schmid, J. M. Silvester, S. Sorella, L. F. Tocchio, L. Wang, S. R. White, A. Wietek, Q. Yang, Y. Yang, S. Zhang, and G. Carleo, *Science* **386**, 296 (2024).
 - [11] A. M. Childs, D. Maslov, Y. Nam, N. J. Ross, and Y. Su, *Proceedings of the National Academy of Sciences* **115**, 9456 (2018).
 - [12] N. Yoshioka, T. Okubo, Y. Suzuki, Y. Koizumi, and W. Mizukami, *npj Quantum Information* **10**, 45 (2024).
 - [13] C. Lyu, X. Xu, M.-H. Yung, and A. Bayat, *Quantum* **7**, 899 (2023).
 - [14] E. Farhi, J. Goldstone, S. Gutmann, and M. Sipser, *arXiv e-prints*, quant-ph/0001106 (2000), [arXiv:quant-ph/0001106 \[quant-ph\]](#).
 - [15] K. Hejazi, M. Motta, and G. K.-L. Chan, *Phys. Rev. Res.* **6**, 033084 (2024).
 - [16] S.-N. Sun, M. Motta, R. N. Tazhigulov, A. T. Tan, G. K.-L. Chan, and A. J. Minnich, *PRX Quantum* **2**, 010317 (2021).
 - [17] H. Nishi, K. Hamada, Y. Nishiyama, T. Kosugi, and Y.-i. Matsushita, *Phys. Rev. Res.* **5**, 043048 (2023).
 - [18] T. Kosugi, Y. Nishiyama, H. Nishi, and Y.-i. Matsushita, *Phys. Rev. Res.* **4**, 033121 (2022).
 - [19] T. Kadowaki and H. Nishimori, *Phys. Rev. E* **58**, 5355 (1998).
 - [20] K. Mitarai, M. Negoro, M. Kitagawa, and K. Fujii, *Phys. Rev. A* **98**, 032309 (2018).
 - [21] M. Motta, C. Sun, A. T. K. Tan, M. J. O’Rourke, E. Ye, A. J. Minnich, F. G. S. L. Brandão, and G. K.-L. Chan, *Nature Physics* **16**, 205 (2020).
 - [22] S. Keller and M. Reiher, *The Journal of Chemical Physics* **144**, 134101 (2016).
 - [23] S. Sharma and G. K.-L. Chan, *The Journal of Chemical Physics* **136**, 124121 (2012).
 - [24] R. Pauncz, *Spin eigenfunctions: construction and use* (Springer Science & Business Media, 2012).
 - [25] J. Planelles and P. Viciano, *Journal of Mathematical Chemistry* **16**, 137 (1994).
 - [26] A. Gandon, A. Baiardi, M. Rossmannek, W. Dobrutz, and I. Tavernelli, *arXiv e-prints*, [arXiv:2412.14797 \(2024\)](#), [arXiv:2412.14797 \[quant-ph\]](#).
 - [27] K. Sugisaki, K. Toyota, K. Sato, D. Shiomi, and T. Takui, *Communications Chemistry* **5**, 84 (2022).
 - [28] K. Seki, T. Shirakawa, and S. Yunoki, *Phys. Rev. A* **101**, 052340 (2020).
 - [29] K. Kuroiwa and Y. O. Nakagawa, *Phys. Rev. Res.* **3**, 013197 (2021).
 - [30] A. Carbone, D. E. Galli, M. Motta, and B. Jones, *Symmetry* **14** (2022), [10.3390/sym14030624](#).
 - [31] D. Lacroix, E. A. Ruiz Guzman, and P. Siwach, *The European Physical Journal A* **59**, 3 (2023).
 - [32] J. R. McClean, S. Boixo, V. N. Smelyanskiy, R. Babbush, and H. Neven, *Nature Communications* **9**, 4812 (2018).
 - [33] H.-N. Xie, S.-J. Wei, F. Yang, Z.-A. Wang, C.-T. Chen, H. Fan, and G.-L. Long, *Phys. Rev. A* **109**, 052414 (2024).
 - [34] T. Liu, J.-G. Liu, and H. Fan, *Quantum Information Processing* **20**, 204 (2021).
 - [35] H. Nishi, T. Kosugi, Y. Nishiyama, and Y.-i. Matsushita, *Phys. Rev. Res.* **6**, L022041 (2024).
 - [36] Y. Nishiyama, H. Nishi, Y. Couzinié, T. Kosugi, and Y.-i. Matsushita, *Phys. Rev. A* **109**, 022423 (2024).
 - [37] P. Siwach and D. Lacroix, *Phys. Rev. A* **104**, 062435 (2021).
 - [38] I. Stetcu, A. Baroni, and J. Carlson, *Phys. Rev. C* **108**, L031306 (2023).
 - [39] D. Lacroix, *Phys. Rev. Lett.* **125**, 230502 (2020).
 - [40] A. M. Childs, Y. Su, M. C. Tran, N. Wiebe, and S. Zhu, *Phys. Rev. X* **11**, 011020 (2021).
 - [41] S. Lloyd, *Science* **273**, 1073 (1996).
 - [42] T. Jahnke and C. Lubich, *BIT Numerical Mathematics* **40**, 735 (2000).
 - [43] I. Kassal, S. P. Jordan, P. J. Love, M. Mohseni, and A. Aspuru-Guzik, *Proceedings of the National Academy of Sciences* **105**, 18681 (2008).
 - [44] H. F. Trotter, *Proceedings of the American Mathematical Society* **10**, 545 (1959).
 - [45] M. Suzuki, *Progress of Theoretical Physics* **56**, 1454 (1976).
 - [46] A. Y. Kitaev, A. Shen, and M. N. Vyalyi, *Classical and quantum computation*, 47 (American Mathematical Soc., 2002).
 - [47] R. Orús, *Annals of Physics* **349**, 117 (2014).
 - [48] W. M. C. Foulkes, L. Mitas, R. J. Needs, and G. Rajagopal, *Rev. Mod. Phys.* **73**, 33 (2001).
 - [49] T. Jones, S. Endo, S. McArdle, X. Yuan, and S. C. Benjamin, *Phys. Rev. A* **99**, 062304 (2019).
 - [50] S. McArdle, T. Jones, S. Endo, Y. Li, S. C. Benjamin, and X. Yuan, *npj Quantum Information* **5**, 75 (2019).
 - [51] X. Yuan, S. Endo, Q. Zhao, Y. Li, and S. C. Benjamin, *Quantum* **3**, 191 (2019).
 - [52] K. Yeter-Aydeniz, R. C. Pooser, and G. Siopsis, *npj Quantum Information* **6**, 63 (2020).
 - [53] S.-H. Lin, R. Dilip, A. G. Green, A. Smith, and F. Pollmann, *PRX Quantum* **2**, 010342 (2021).
 - [54] R. Meister and S. C. Benjamin, *arXiv e-prints*, [arXiv:2212.00846 \(2022\)](#), [arXiv:2212.00846 \[quant-ph\]](#).
 - [55] S. Shirai, H. Iwakiri, K. Kanno, T. Horiba, K. Omiya, H. Hirai, and S. Koh, *ACS Omega* **8**, 19917 (2023).
 - [56] P.-O. Löwdin and O. Goscinski, *International Journal of Quantum Chemistry* **4**, 533 (1969).
 - [57] J. Kattemölle and J. van Wezel, *Phys. Rev. B* **106**, 214429 (2022).
 - [58] X. Yi, J. Huo, G. Liu, L. Fan, R. Zhang, and C. Cao, *EPJ Quantum Technology* **12**, 43 (2025).
 - [59] S. Moudgalya, N. Regnault, and B. A. Bernevig, *Phys.*

- Rev. B **98**, 235156 (2018).
- [60] N. F. Chilton, *Annual Review of Materials Research* **52**, 79 (2022).
- [61] F. H. Essler, H. Frahm, F. Göhmann, A. Klümper, and V. E. Korepin, *The one-dimensional Hubbard model* (Cambridge University Press, 2005).
- [62] A. Rajca, *Chemical Reviews* **94**, 871 (1994).
- [63] E. Wigner, *Pure and applied physics* (2012).
- [64] W. Zi, J. Nie, and X. Sun, *arXiv e-prints*, arXiv:2404.06052 (2024), arXiv:2404.06052 [quant-ph].
- [65] R. P. Stanley, *Catalan numbers* (Cambridge University Press, 2015).
- [66] M. Mootz, P. P. Orth, C. Huang, L. Luo, J. Wang, and Y.-X. Yao, *Quantum Science and Technology* **9**, 035054 (2024).
- [67] N. P. D. Sawaya, T. Menke, T. H. Kyaw, S. Johri, A. Aspuru-Guzik, and G. G. Guerreschi, *npj Quantum Information* **6**, 49 (2020).
- [68] A. Javadi-Abhari, M. Treinish, K. Krsulich, C. J. Wood, J. Lishman, J. Gacon, S. Martiel, P. D. Nation, L. S. Bishop, A. W. Cross, B. R. Johnson, and J. M. Gambetta, “Quantum computing with Qiskit,” (2024), arXiv:2405.08810 [quant-ph].
- [69] D. Kouzoudis, *Journal of Magnetism and Magnetic Materials* **173**, 259 (1997).
- [70] H. Hu and B. Wu, *Phys. Rev. A* **93**, 012345 (2016).
- [71] K. N. Ferreira, T. M. Iverson, K. Maghlaoui, J. Barber, and S. Iwata, *Science* **303**, 1831 (2004).
- [72] D. N. Hendrickson, G. Christou, E. A. Schmitt, E. Libby, J. S. Bashkin, S. Wang, H. L. Tsai, J. B. Vincent, and P. D. W. Boyd, *Journal of the American Chemical Society* **114**, 2455 (1992).
- [73] H. Isobe, M. Shoji, K. Koizumi, Y. Kitagawa, S. Yamanaka, S. Kuramitsu, and K. Yamaguchi, *Polyhedron* **24**, 2767 (2005), proceedings of the 9th International Conference on Molecule-based Magnets (ICMM 2004).
- [74] S. Gocho, H. Nakamura, S. Kanno, Q. Gao, T. Kobayashi, T. Inagaki, and M. Hatanaka, *npj Computational Materials* **9**, 13 (2023).
- [75] H. Nishi, Y. Takei, T. Kosugi, S. Mieda, Y. Natsume, T. Aoyagi, and Y.-i. Matsushita, *arXiv e-prints*, arXiv:2407.10555 (2024), arXiv:2407.10555 [quant-ph].
- [76] H. Ma, M. Govoni, and G. Galli, *npj Computational Materials* **6**, 85 (2020).
- [77] A. Roggero, C. Gu, A. Baroni, and T. Papenbrock, *Phys. Rev. C* **102**, 064624 (2020).
- [78] K. M. Nakanishi, K. Mitarai, and K. Fujii, *Phys. Rev. Res.* **1**, 033062 (2019).
- [79] O. Higgott, D. Wang, and S. Brierley, *Quantum* **3**, 156 (2019).
- [80] I. Kassal, S. P. Jordan, P. J. Love, M. Mohseni, and A. Aspuru-Guzik, *Proceedings of the National Academy of Sciences* **105**, 18681 (2008).
- [81] N. C. Jones, J. D. Whitfield, P. L. McMahon, M.-H. Yung, R. V. Meter, A. Aspuru-Guzik, and Y. Yamamoto, *New Journal of Physics* **14**, 115023 (2012).
- [82] T. Kosugi, H. Nishi, and Y.-i. Matsushita, *npj Quantum Information* **9**, 112 (2023).

Appendix A: Binary encoding of $S = 5/2$ and $S = 2$ Spin states

Here, we present the explanation of the binary encoding for $S = 5/2$ and $S = 2$, which is used in numerical experiments of the manganese trimer. There are several methods to encode high-spin states, such as Gray encoding, but in this paper, we used the standard binary encoding. In the standard binary encoding, the transformation from original states to encoded states is summarized in Tab. I.

Spin state	Encoded	Spin state	Encoded
$ 5/2, 5/2\rangle$	$ 000\rangle$	$ 2, 2\rangle$	$ 000\rangle$
$ 5/2, 3/2\rangle$	$ 001\rangle$	$ 2, 1\rangle$	$ 001\rangle$
$ 5/2, 1/2\rangle$	$ 010\rangle$	$ 2, 0\rangle$	$ 010\rangle$
$ 5/2, -1/2\rangle$	$ 011\rangle$	$ 2, -1\rangle$	$ 011\rangle$
$ 5/2, -3/2\rangle$	$ 100\rangle$	$ 2, -2\rangle$	$ 100\rangle$
$ 5/2, -5/2\rangle$	$ 101\rangle$		

TABLE I: Binary encoding representation of $S = 5/2$ and $S = 2$ Spin states.

The spin operators are also rewritten. The encoded spin operators for $S = 5/2$ can be written as follows. In this

appendix, for the sake of clarity in notation, Pauli matrices σ_{ix} , σ_{iy} , and σ_{iz} are written as X_i , Y_i , and Z_i , respectively.

$$S_x = \frac{3 + 2\sqrt{5}}{8}X_0 + \frac{-3 + 2\sqrt{5}}{8}Z_1X_0 + \frac{3}{8}(Z_2X_0 - Z_2Z_1X_0) + \frac{1}{\sqrt{8}}(X_1X_0 + Y_1Y_0 + X_2X_1X_0 - X_2Y_1Y_0 + Y_2X_1Y_0 + Y_2Y_1X_0 + Z_2X_1X_0 + Z_2Y_1Y_0) \quad (\text{A1})$$

$$S_y = \frac{3 + 2\sqrt{5}}{8}Y_0 + \frac{-3 + 2\sqrt{5}}{8}Z_1Y_0 + \frac{3}{8}(Z_2Y_0 - Z_2Z_1Y_0) + \frac{1}{\sqrt{8}}(Y_1X_0 - X_1Y_0 - Y_2Y_1Y_0 + Y_2X_1X_0 - X_2Y_1X_0 - X_2X_1Y_0 + Z_2Y_1X_0 - Z_2X_1Y_0) \quad (\text{A2})$$

$$S_z = \frac{1}{8}(Z_2Z_0 + Z_1Z_0 - Z_2Z_1Z_0) + \frac{3}{8}Z_0 + (Z_2 + Z_2Z_1) \quad (\text{A3})$$

The encoded spin operators for $S = 2$ can be written like

$$S_x = \frac{1 + \sqrt{3/2}}{4}(X_0 + Z_2X_0) + \frac{1 - \sqrt{3/2}}{4}(Z_1X_0 + Z_2Z_1X_0) + \frac{\sqrt{3/2}}{4}(X_1X_0 + Y_1Y_0 + Z_2X_1X_0 + Z_2Y_1Y_0) + \frac{1}{4}(X_2X_1X_0 - X_2Y_1Y_0 + Y_2X_1Y_0 + Y_2Y_1X_0) \quad (\text{A4})$$

$$S_y = \frac{1 + \sqrt{3/2}}{4}(Y_0 + Z_2Y_0) + \frac{1 - \sqrt{3/2}}{4}(Z_1Y_0 + Z_2Z_1Y_0) + \frac{\sqrt{3/2}}{4}(Y_1X_0 - X_1Y_0 + Z_2Y_1X_0 - Z_2X_1Y_0) + \frac{1}{4}(Y_2X_1X_0 - X_2X_1Y_0 - X_2Y_1X_0 - Y_2Y_1Y_0) \quad (\text{A5})$$

$$S_z = \frac{1}{4}(Z_1 - Z_1Z_0 + Z_2Z_1Z_0) + \frac{1}{2}(Z_2 + Z_2Z_0) + \frac{3}{4}Z_2Z_1 \quad (\text{A6})$$

Note that in the numerical experiments, the evaluation does not reveal any differences in the results due to the choice of encoding method, even though the encoding affects the number of qubits, gate complexity, and robustness to qubit noise.